A Genuine Demonstration of the Radiative Greenhouse Effect

Claudiu Saftoiu[1,*]

April 13, 2026

[1]Independent Researcher, Portugal 8400-556

[*]Corresponding author: Claudiu Saftoiu
E-mail: csaftoiu@gmail.com

Keywords: greenhouse effect, experimental demonstration, radiative heat transfer

Abstract

Despite its central importance to understanding the Earth's climate, experimental demonstrations of the radiative greenhouse effect are surprisingly lacking, with many purported tabletop demonstrations inadvertently illustrating other, non-radiative mechanisms. A set of controlled experiments has been devised to close this critical gap. By covering a sky-exposed black surface with panes of differing optical materials, it is shown that panes that are more opaque to infrared radiation causally result in a warmer surface temperature than those more transmissive of it. Systematic control experiments confirmed the radiative nature of the observed temperature differences, ruling out confounding factors. A variant of the experiment is provided which is performable in under an hour. A simple computer model is also made available which closely matches experimental results and may prove useful for illustrating the heat flows involved.

1 Introduction

The greenhouse effect is a well-understood radiative phenomenon by which the atmosphere's transparency to sunlight yet selective absorption and emission of infrared light results in the Earth's surface being warmer than it otherwise would be without this radiative emission [1]. As it is central to understanding the Earth's climate, a tangible demonstration would be a wonderful boon to teaching students about the effect. However, this currently proves to be a challenge. Actual greenhouses do not serve as an example, as they mostly stay warm due to their walls physically preventing the sun-heated air inside from escaping rather than any radiative effects [2]. Neither the historical literature[1] nor the modern literature[2] provide an experiment that actually demonstrates a surface's temperature increasing due to the greenhouse effect, with certain modern table-top demonstrations that use carbon dioxide actually functioning due to convective rather than radiative effects [11, 12]. This article presents a novel experiment to fill this critical gap, along with a variant that is easy to perform in under an hour.

2 Experimental design

The experiment entails using three identical copies of a specially-designed 3D-printed apparatus. Its design visually exposes a 40 mm diameter black surface, allowing placement of a 2 mm thick optical pane above it separated by a 1 mm air gap. The apparatus allows placement of a thermocouple immediately underneath the black surface to measure its temperature.

Three optical materials were used: borosilicate [13], sapphire [14], and calcium fluoride [15] (CaF_2). Their material properties are listed in Table 1. Their solar and infrared properties were measured with a pyranometer and pyrgeometer placed in modified apparatus housings. The materials are each highly transparent to sunlight yet have differing infrared transmittances, with borosilicate being the most infrared-opaque and calcium fluoride the most transmissive (Figure 1). As plain borosilicate is less transmissive of sunlight than calcium fluoride, the borosilicate pane had a 400-1000 nm anti-reflective coating applied to both sides to bring its solar transmittance closer to, while still remaining lower than, that of calcium fluoride.

The apparatuses were placed on the rooftop of a house to maximize their exposure to the sky (Figure 2). They were placed on top of individual solar plate levelers to ensure identical solar inclination and thus insolation entering the apertures, which was confirmed with a pyranometer at the start of each run. Control experiments determined there were minimal differences between the apparatuses. However, their relative placement to each other had a noticeable effect, which was

[1] Tyndall [3] demonstrated carbon dioxide's infrared-absorbing potential, but not this property leading to a warmer surface temperature. Foote [4] showed CO_2's solar-absorbing potential, whereas the greenhouse effect is driven by its capacity to absorb long-wave infrared radiation. Wood [5] performed a similar experiment to the one in this paper, yet found essentially a null result, *i.e.* no significant surface warming effect.

[2] Levendis [6] showed a delayed cooling effect, rather than a warming effect. Halpern [7] used an electric resistance heating element as a heat source rather than sunlight. This is a meaningful distinction: a key aspect of the greenhouse effect is that the atmosphere is transparent to solar radiation yet partially opaque to infrared radiation, and recent research on absorbing aerosols shows that increasing the atmosphere's opacity to sunlight results in surface cooling rather than warming [8, 9]. Blume [10] detailed various experiments, however they do not account for convective suppressive effects, and while they demonstrate carbon dioxide's absorptive properties as Tyndall did, they only show this resulting in the gas itself increasing in temperature, rather than a sun-exposed surface.

apparently due to the different convection patterns in the different positions. To account for this, six trials for each of the six possible permutations of the panes were run, with the results averaged. This enabled comparing the effect of the more infrared-transparent panes versus the more infrared-opaque ones on the surface temperatures. The experiments were run for 24 hours to determine the effect across all hours of the day and night.

Extended details of the apparatus design, placement, and solar transmission and infrared loss measurements are available in the Supplementary Materials (SM) Section 2.

3 Experimental results

Results from all six combinations under mostly clear-sky conditions are aggregated together and displayed in Figure 3 and summarized in Table 2. The surfaces remained significantly hotter when they were under the borosilicate pane than under the calcium fluoride pane, across all combinations. Further, the difference was higher during peak sunlight hours, with several individual runs peaking at a 3.5 °C difference. Notably, this temperature difference occurred even though the borosilicate-covered surfaces received less solar insolation than calcium-fluoride-covered ones (Table 1). When under the sapphire pane, surfaces similarly remained warmer despite receiving almost 10% less insolation than the surface through the calcium fluoride pane.

The higher average temperature persisted across nighttime as well, despite a small dip for the borosilicate during indirect sunlight hours. Unexpectedly, the sapphire pane resulted in a higher temperature than the borosilicate at night, despite being more transparent to infrared. This was determined to be due to sapphire's reduced infrared emissivity causing it to radiate heat more slowly to the night sky as compared to borosilicate (SM Section 5.6).

The temperature differences persisted during cloudy conditions as well (Figure 4). The data is far more chaotic, but on average, borosilicate demonstrated superior heat retention.

All raw data, several additional figures, and a two-pane variant of the experiment are available in SM Section 3.

4 Simplified variant

For live demonstration purposes, a simplified variant is presented which highlights the causality of the effect. It uses only the borosilicate and calcium fluoride panes, was performed at ground level rather than on a rooftop, and provides alternatives to the pyranometer and pyrgeometer measurements.

The procedure is:

1. Set up the apparatuses on a flat, level surface, outdoors, on a sunny, clear-sky day.

2. Demonstrate the differing infrared properties of the panes. This can be done either with a pyrgeometer showing different reductions in net infrared loss to the sky with the panes in place, or with a hand-held infrared thermometer if one is not available (Section 4.1).

3. Without any panes in place, let the apparatuses heat up until a roughly steady-state. They will become significantly warmer than the outside air. Their temperatures will be close to

each other but may show small variations caused by local environmental changes, such as drafts of wind (Figure 5a).

4. Insert the calcium fluoride into one apparatus and the borosilicate into the other. Let the temperatures evolve for 10-15 minutes. The surface under the borosilicate will become warmer than under the calcium fluoride (Figure 5b).

5. Swap the optical panes. The surface that was under the calcium fluoride before the swap is now under the borosilicate; it will go from being the cooler to being the warmer of the two surfaces (Figure 5c).

6. Rule out differences in solar transmissivity as a cause for the effect by demonstrating that borosilicate transmits less sunlight than calcium fluoride. This can be done either with a pyranometer directly measuring the solar insolation through the panes, or with a regular pane of glass (see Section 4.2).

4.1 Handheld infrared thermometer readings

The intended use of an infrared thermometer is to read the temperature of the object it's pointing at. This can be demonstrated by pointing it at one's skin or a bowl of ice water. However, when pointed at the clear sky, the display will show a very cold temperature (*e.g.* -20 °C). This is not an accurate temperature measurement (and the sky does not have only one temperature, as it varies with altitude). Rather, the infrared thermometer functions by measuring the net radiative heat transfer between itself and whatever is in its view, then computing what a graybody's temperature would have to be to yield that same measurement. The below-zero temperature reading merely indicates that the sensor is losing a significant amount of infrared radiation to the sky, *i.e.* it is receiving far less radiation back than it is emitting. It's relevant to note that if the sky did not absorb or emit any infrared radiation at all, the thermometer would theoretically read close to the temperature of outer space (around -276 °C).

This property can be exploited to demonstrate the infrared properties of the panes. By keeping the handheld thermometer pointed upwards, yet holding a pane between the sensor and the sky, the thermometer now reads the amount of radiation it's receiving back from the pane itself, in combination with whatever is filtered through from the sky behind it. As borosilicate is nearly completely opaque to infrared, it fully obscures the sky behind it across these wavelengths, and the infrared thermometer will end up showing the temperature of the borosilicate pane itself (*e.g.* +17 °C). As calcium fluoride is partly transparent to infrared, the thermometer ends up reading a temperature somewhere between what it gave for the sky and the borosilicate (*e.g.* -2 °C). These readings indicate that with the calcium fluoride pane in place, the infrared thermometer's sensor loses less heat radiatively to the sky than without any pane in place, but loses more heat than with the borosilicate pane in place.

4.2 Demonstrating solar transmissivity with a pane of glass

The relative solar transmittance of the panes can be demonstrated by removing the panes from the apparatuses and placing a large plate of regular glass on top of the apparatuses, covering both of them at once. Then, place the optical panes *on top of* the pane of glass, allow the temperatures to

evolve (Figure 6a), and swap their positions after about 10-15 minutes. The temperature behavior will be reversed, where the surface under the calcium fluoride now remains the hotter of the two (Figure 6b).

The reason is that regular glass is fully opaque to infrared, and thus equalizes both apparatuses in terms of their surfaces' infrared exchange with the sky. Placing the optical panes above the plate of glass does not significantly alter the surface's infrared exchange with the sky, thus making the panes behave essentially as solar filters. As the calcium fluoride is more transmissive than the borosilicate, the surface under the calcium fluoride remains warmer.

5 Discussion

The radiative greenhouse effect explains the experimental results: the surfaces are warmed by the sunlight as filtered through the panes, and lose heat radiatively to the sky. Under the borosilicate and sapphire panes, the surface's rate of radiative heat loss is reduced as compared to when under the calcium fluoride pane, which leads to a measurably significant warming effect during both day and night. Non-radiative confounding factors can be systematically ruled out:

Solar Transmissivity. The solar transmissive properties of the panes are critical. If calcium fluoride simply blocked more sunlight, the reduced energy input could explain its cooler surface. However, calcium fluoride transmitted the *most* sunlight yet still produced the coolest surface, demonstrating that the greenhouse effect from the borosilicate and sapphire overcame their reduced solar input.

Construction, Positioning, and Environment. The results come from averaging together six runs, covering all possible combinations placing the three panes in the apparatuses. These averaged results rule out the possibility that the cause is either systemic differences or transient interactions between the apparatuses and the environment, and the consistency of the measurements indicates the magnitude of the temperature differences is significant. For the simplified variant, the temperature evolution changes as soon as the panes are added and swapped, indicating a clear causal effect that is unlikely to coincide with an unrelated environmental change. The panes can be swapped multiple times to provide further evidence that the effect is unrelated to coincidental environmental changes, or left to evolve longer to show greater temperature differences.

Convection. Convective loss from the surface to the pane is fully suppressed due to the small, 1 mm air gap (Rayleigh number $\ll$ the critical value [16]), meaning only conduction occurs across the gap. Although the panes and the apparatus exteriors still exchange heat convectively with the outside air, the nature of the convection is the same for both apparatuses, and swaps in positioning rule out transient or systemic environmental factors.

Other Thermal Properties. Borosilicate is less thermally conductive and has a smaller heat capacity than calcium fluoride, while sapphire has higher values for both properties, yet the surfaces remained warmer under both of these panes. Control experiments performed with aluminum and acrylic indicated borosilicate's lower conductance has a small but negligible effect, and the different heat capacities have essentially no effect (SM Section 5.4).

6 Model

A model is presented to help illustrate the physics at play. Using physically plausible simplifying assumptions and material values, the model produced output highly congruent with experimental measurements, supporting both steady-state analysis (Section 6.1) and time-evolution modelling (Section 6.2).

The approach models temperatures of the black exposed surface T_{surf} and optical pane T_{pane} isothermally. At each time-step the model takes as input the ambient air temperature T_∞, insolation I_{sun}, and sky backradiation I_{sky} from instrument measurements, and uses coupled conductive, convective, and radiative heat transfer to update internal energies:

$$\frac{dU_{\text{surf}}}{dt} = Q_{\text{cond,surf}\to\infty} + Q_{\text{cond,surf}\to\text{pane}} + Q_{\text{sun,surf}} + Q_{\text{rad,surf}} \tag{1}$$

$$\frac{dU_{\text{pane}}}{dt} = Q_{\text{cond,pane}\to\text{surf}} + Q_{\text{conv,pane}\to\infty} + Q_{\text{sun,pane}} + Q_{\text{rad,pane}} \tag{2}$$

The key heat transfer equations are summarized in Table 3. Full derivations, parameter values, and more thorough explications of the heat flows are provided in SM Section 6, and the Python source code is publicly available.

6.1 Steady-state results

Table 4 presents the steady-state model outputs alongside measured values from one of the experimental runs. The temperature ranking is correct for both daytime (borosilicate hottest) and nighttime (sapphire hottest), with close agreement in absolute and relative temperatures.

Peak Sunlight Analysis. Although the surface under borosilicate receives less sunlight than under calcium fluoride, it remains warmer. The reason is that its radiative loss $Q^{\circ}_{\text{rad,surf}}$ is even smaller than the reduction in sunlight. The key is $Q^{\circ}_{\text{rad,surf}\leftarrow\text{pane}}$: the surface gains 70 W/m^2 more energy from the borosilicate pane's downward infrared emission than from CaF_2's downward emission plus sky transmission. This, then, is the radiative greenhouse effect.

Nighttime Analysis. The model reproduces the nighttime behavior where surfaces remain 1–2° cooler than the ambient air. Both surfaces and panes lose heat radiatively to the cooler night sky, offset by conductive and convective gains from ambient air. The surface under CaF_2 loses the most heat radiatively and ends up coolest. Borosilicate and sapphire retain surface heat roughly equally, but the borosilicate pane loses more heat to the sky, yielding a cooler surface than sapphire.

6.2 Time-series validation

The model was validated against the time-series data from six experimental runs. Relative temperature differences matched closely, and absolute temperatures agreed within 1°C at night and 3°C during daytime. The modelled transition in temperature ranking (sapphire hottest at night transitioning to borosilicate hottest during day) closely matched the measured timing around 9AM.

7 Conclusion

The experiment detailed in this article closes a critical gap in causally demonstrating the greenhouse effect. It is simple to perform, and the radiative nature of the effect is thoroughly validated by supporting experiments. A model is presented which corroborates the analysis and elucidates the heat flows involved. A valuable pedagogical tool is thus now available and able to be added to appropriate curricula.

References

[1] M.D.H. Jones and A. Henderson-Sellers. History of the greenhouse effect. *Progress in Physical Geography*, 14(1):1–18, 1990. URL: https://www.crcresearch.org/sites/default/files/u11276/historyofgreenhousegaseffect.pdf, doi:10.1177/030913339001400101.

[2] IPCC. Historical overview of climate change science. In S. Solomon, D. Qin, M. Manning, Z. Chen, M. Marquis, K.B. Averyt, M. Tignor, and H.L. Miller, editors, *Climate Change 2007: The Physical Science Basis. Contribution of Working Group I to the Fourth Assessment Report of the Intergovernmental Panel on Climate Change*, chapter 1, page 115. Cambridge University Press, Cambridge, United Kingdom and New York, NY, USA, 2007.

[3] J. Tyndall. On the transmission of heat of different qualities through gases of different kinds. *Proceedings of the Royal Institution*, 3:155–158, 1859.

[4] Eunice Foote. Circumstances affecting the heat of the sun's rays. *American Journal of Science and Arts*, pages 117–118, 1856.

[5] R.W. Wood. Xxiv. note on the theory of the greenhouse. *The London, Edinburgh, and Dublin Philosophical Magazine and Journal of Science*, 17(98):319–320, 1909. doi:10.1080/14786440208636602.

[6] Yiannis A. Levendis, Gregory Kowalski, Yang Lu, and Gregory Baldassarre. A simple experiment on global warming. *Royal Society Open Science*, 7(9):192075, 2020. URL: https://royalsocietypublishing.org/doi/10.1098/rsos.192075, doi:10.1098/rsos.192075.

[7] J. B. Halpern. R w wood's experiment done right – a laboratory demonstration of the greenhouse effect. In *AGU Fall Meeting Abstracts*, volume 2016, pages ED21A–0767, 2016. URL: https://ui.adsabs.harvard.edu/abs/2016AGUFMED21A0767H/abstract.

[8] R. Krishnan and V. Ramanathan. Evidence of surface cooling from absorbing aerosols. *Geophysical Research Letters*, 29(9):54–1–54–4, 2002. URL: https://agupubs.onlinelibrary.wiley.com/doi/abs/10.1029/2002GL014687, arXiv:https://agupubs.onlinelibrary.wiley.com/doi/pdf/10.1029/2002GL014687, doi:10.1029/2002GL014687.

[9] Geeta G. Persad, David J. Paynter, Yi Ming, and V. Ramaswamy. Competing atmospheric and surface-driven impacts of absorbing aerosols on the east asian summertime climate. *Journal of Climate*, 30(22):8929 – 8949, 2017. URL: https://journals.ametsoc.org/view/journals/clim/30/22/jcli-d-16-0860.1.xml, doi:10.1175/JCLI-D-16-0860.1.

[10] Bernd Blume and Klaus Morgenstern. *Global warming and climate change – an experimental approach*. CarboEurope, 2015. URL: https://www.carboeurope.org/wp-content/uploads/2024/06/Bernd-BlumeExperiments.pdf.

[11] Paul Wagoner, Chunhua Liu, and R. G. Tobin. Climate change in a shoebox: Right result, wrong physics. *American Journal of Physics*, 78(5):536–540, 05 2010. arXiv:https://pubs.aip.org/aapt/ajp/article-pdf/78/5/536/13095812/536_1_online.pdf, doi:10.1119/1.3322738.

[12] Jerry A. Bell. Benchtop global-warming demonstrations do not exemplify the atmospheric greenhouse effect, but alternatives are available. *Journal of Chemical Education*, 96(10):2352–2354, 2019. doi:10.1021/acs.jchemed.8b01057.

[13] Knight Optical (UK) Limited. Technical / sheet glasses — SCHOTT BOROFLOAT® 33 (tsg-legb), 2020. URL: https://www.knightoptical.com/wp-content/uploads/2020/01/Sheet-Glass-Borofloat33-TSG-LEGB.pdf.

[14] Knight Optical (UK) Limited. Optical material / crystals (infrared) — sapphire (c-cut, uv), 2020. URL: https://www.knightoptical.com/wp-content/uploads/2020/02/IR-material-Sapphire_C-cut_UV.pdf.

[15] Knight Optical (UK) Limited. Infrared optics — calcium fluoride (caf_2), 2025. URL: https://www.knightoptical.com/wp-content/uploads/2020/02/Datasheet-IR-Material-Calcium-Fluoride.pdf.

[16] P. L. Silveston. Wärmedurchgang in waagerechten Flüssigkeitsschichten. *Forschung auf dem Gebiet des Ingenieurwesens A*, 24(1):29–32, 1958. doi:10.1007/BF02557078.

[17] Präzisions Glas & Optik GmbH. BOROFLOAT® | transmission curve | thickness 2 mm, 2025. URL: https://www.pgo-online.com/intl/curves/boro_kurve.html.

[18] Courtesy of Edmund Optics. Sapphire windows, 2025. URL: https://www.edmundoptics.com/f/sapphire-windows/12234/.

[19] IMPEX HighTech GmbH. Caf_2 — calcium fluoride, 2025. URL: https://www.impex-hightech.de/en/caf2/.

[20] ASTM International. Standard tables for reference solar spectral irradiances: Direct normal and hemispherical on 37° tilted surface (data provided by the u.s. department of energy, national renewable energy laboratory, operated by alliance for sustainable energy, llc). Technical Report G173-03(2023), American Society for Testing and Materials, West Conshohocken, PA, 2023. URL: https://www.nrel.gov/grid/solar-resource/spectra-am1.5.html.

[21] M. J. Assael, S. Botsios, K. Gialou, and I. N. Metaxa. Thermal conductivity of polymethyl methacrylate (PMMA) and borosilicate crown glass BK7. *International Journal of Thermophysics*, 26(5):1595–1605, 2005. doi:10.1007/s10765-005-8106-5.

[22] SCHOTT AG. Schott borofloat 33 borosilicate float glass data sheet, n.d. URL: https://psec.uchicago.edu/glass/borofloat_33_e.pdf.

[23] Yuan-Yuan Qi, Tian Zhang, Yan Cheng, Xiang-Rong Chen, Dong-Qing Wei, and Ling-Cang Cai. Lattice dynamics and thermal conductivity of calcium fluoride via first-principles investigation. *Journal of Applied Physics*, 119(9):095103, 03 2016. arXiv:https://pubs.aip.org/aip/jap/article-pdf/doi/10.1063/1.4942841/13437927/095103_1_online.pdf, doi:10.1063/1.4942841.

[24] Y. S. Touloukian and C. Y. Ho. *Thermophysical Properties of Matter, Volume 2: Thermal Conductivity - Nonmetallic Solids*. IFI/Plenum, New York, 1970.

[25] D. E. Groom. Atomic and nuclear properties of materials. Technical report, Lawrence Berkeley National Laboratory, 1998.

[26] Jason M. Lonergan, Charmayne Lonergan, Joshua Silverstein, Pornsinee Cholsaipant, and John McCloy. Thermal properties of sodium borosilicate glasses as a function of sulfur content. *Journal of the American Ceramic Society*, 103:3610–3619, 2020. doi:10.1111/jace.17057.

[27] Malcolm W. Chase. Nist-janaf thermochemical tables. Technical Report Monograph No. 9, National Institute of Standards and Technology, Gaithersburg, MD, 1998.

[28] National Center for Biotechnology Information. Calcium fluoride - pubchem compound summary, 2025. URL: https://pubchem.ncbi.nlm.nih.gov/compound/Calcium-Fluoride.

[29] John W. Anthony, Richard A. Bideaux, Kenneth W. Bladh, and Monte C. Nichols. Corundum, mineral data publishing. Handbook of Mineralogy, 2001. URL: https://handbookofmineralogy.org/pdfs/corundum.pdf.

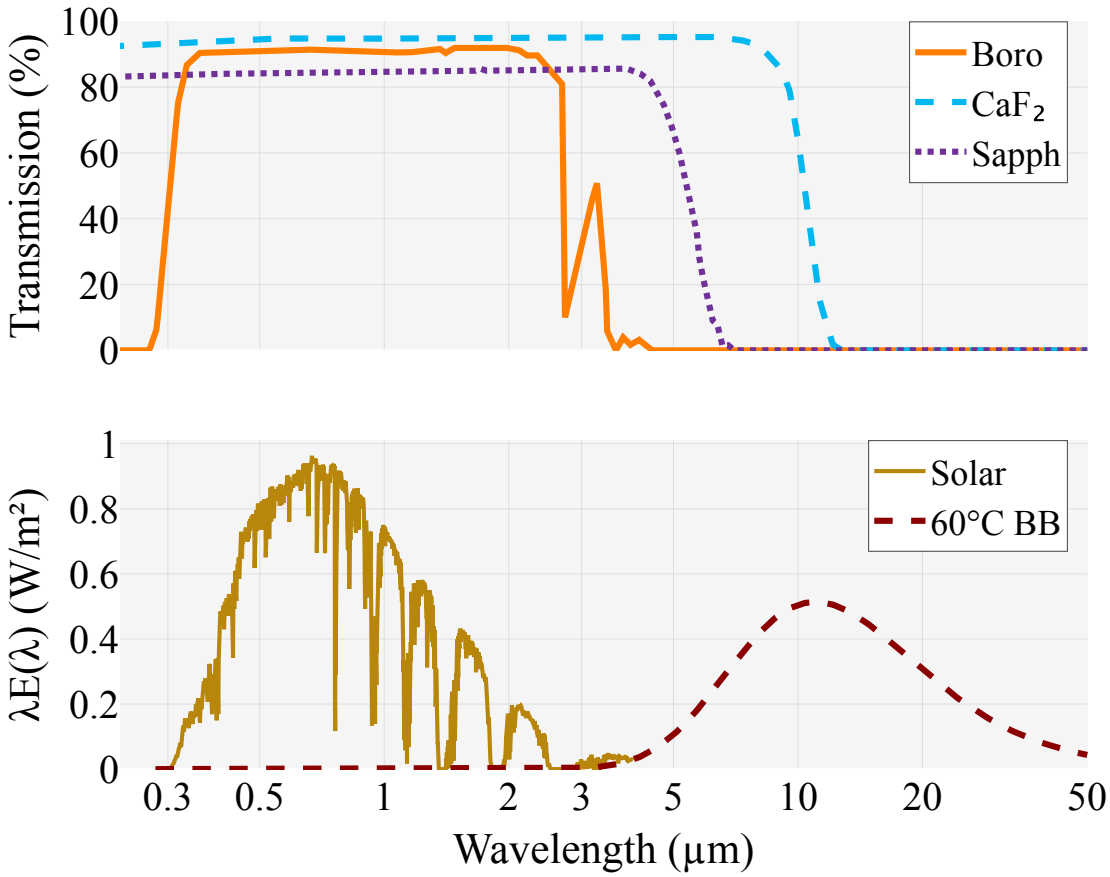

Figure 1: Top. Transmission spectra of 2 mm thick borosilicate, sapphire, and calcium fluoride [17–19] across solar and infrared wavelengths. **Bottom.** Spectral distribution of solar irradiance (ASTM G-173 global tilt [20]) and 60 °C blackbody exitance, plotted as $\lambda E(\lambda)$ such that visual area under each curve corresponds to total power. All three materials are highly transparent to sunlight but differ markedly in infrared transmittance, with borosilicate transmitting almost none of the blackbody spectrum, while calcium fluoride remaining transparent to a significant portion of it.

(a) Experimental setup on the roof showing (from background to foreground): pyrgeometer, apparatuses A, B, and C, and pyranometer. The air temperature sensor housing is visible in the foreground corner.

(b) Sky view from the apparatus location, facing east during morning hours, demonstrating unobstructed sky exposure.

Figure 2: Experimental apparatus placement and sky exposure.

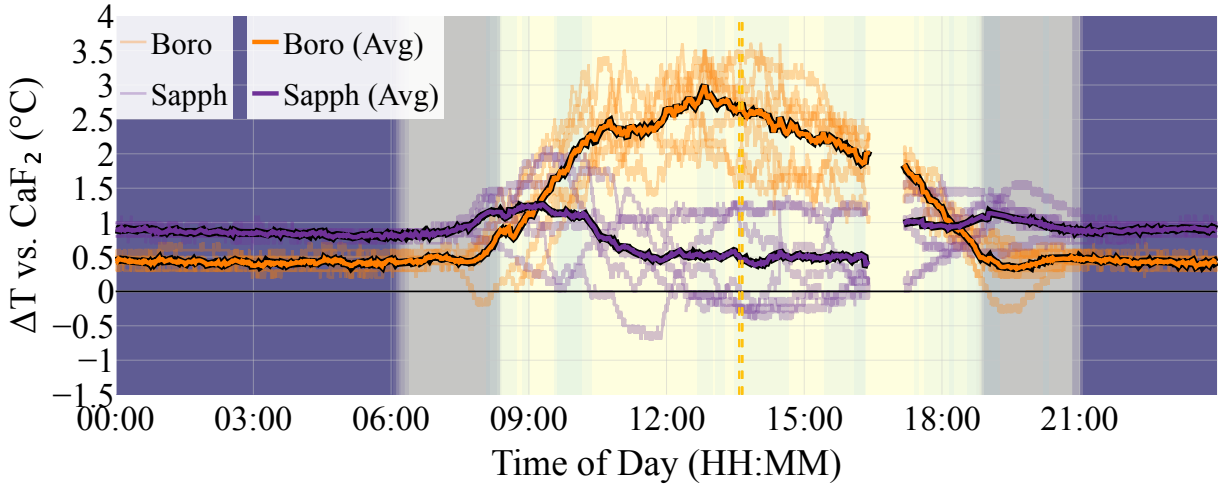

Figure 3: Clear-sky temperature differences between surfaces under infrared-opaque panes (borosilicate and sapphire) vs. infrared-transparent panes (calcium fluoride). The former maintained consistently warmer surfaces underneath. Each semi-transparent trace represents an experimental run, while bold lines show averages. Background shading indicates nighttime (dark blue), indirect sunlight (gray), and direct sunlight (yellow). Light blue overlay marks periods when clouds were present during some experimental runs.

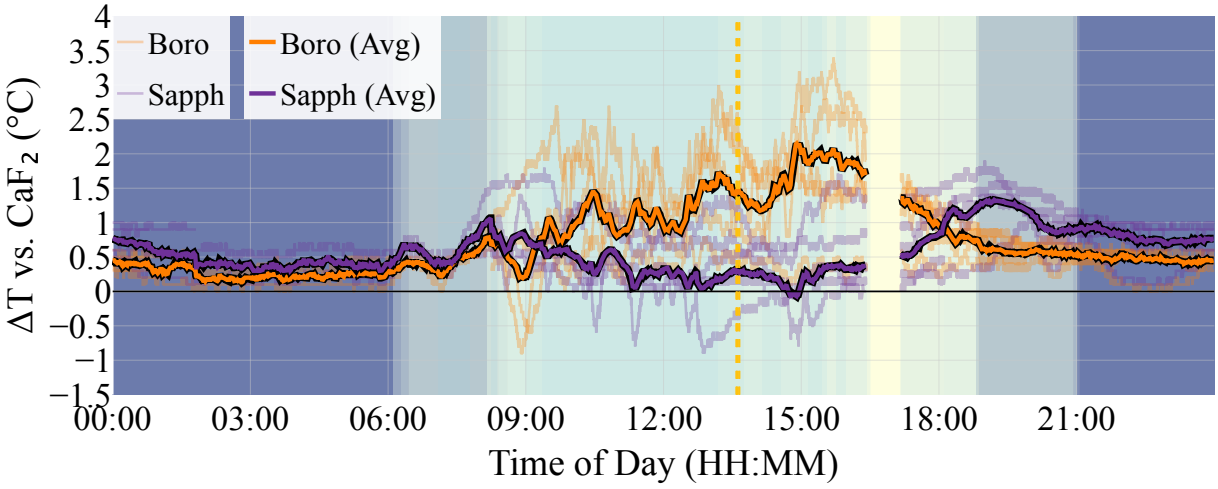

Figure 4: Temperature differences for cloudy conditions showing persistent temperature advantage of infrared-opaque over infrared-transparent panes. Display format matches Figure 3. Includes only data from combinations BCS (i.e. Boro in A, CaF_2 in B, and Sapphire in C), CSB, and SCB, with three averaged runs for CSB.

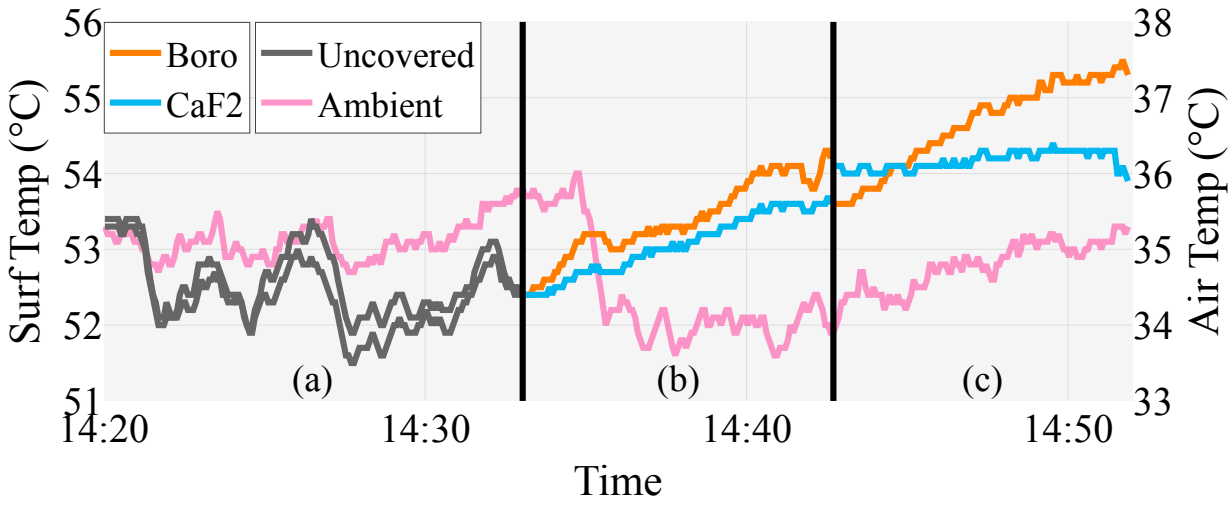

Figure 5: Experimental run of the simple variant. (a) Apparatuses start uncovered. Temperatures are closely coupled and largely follow the variations in ambient air temperature. (b) The panes are placed. Both temperatures rise, but the surface under the borosilicate remains hotter. (c) The panes are swapped. The temperatures now reverse rank; the same surface that was cooler under the calcium fluoride now becomes hotter under the borosilicate.

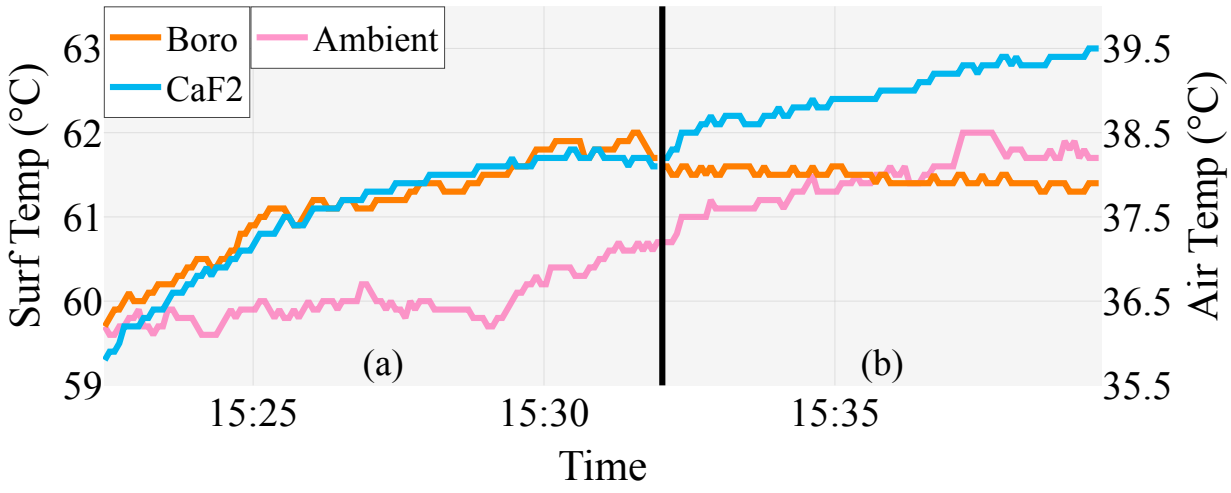

Figure 6: Solar transmittance demonstration with glass pane. (a) Temperatures with plate glass in place and panes sitting on top of the glass. (b) The panes on top are swapped. The surface under the calcium fluoride now becomes clearly hotter. This behavior indicates greater solar transmittance for the calcium fluoride, with an offsetting transient environmental benefit for one of the apparatuses.

	Borosilicate		**Sapphire**		**CaF_2**	
	min	max	min	max	min	max
Solar Transmission (1PM)	90.0%	90.9%	83.2%	83.7%	91.4%	92.2%
Solar Transmission (6PM)	79.7%	81.5%	78.3%	80.1%	84.2%	86.2%
Infrared Loss (2PM, ∼40/air °C)	7.5%	8.3%	10.2%	11.2%	56.5%	58.6%
Infrared Loss (2PM, ∼40/39-42 °C)	0.0%	0.0%	1.4%	2.3%	44.6%	47.1%
Infrared Loss (6PM, ∼30/air °C)	0.0%	1.5%	0.0%	0.3%	41.9%	44.7%
Infrared Loss (9PM, ∼28/air °C)	0.0%	3.7%	0.0%	4.9%	40.9%	43.4%
Thermal Conductivity (W/(m·K))	1.1	1.2	18.7	33.0	9.7	10.8
Heat Capacity (J/K)	7.0	8.9	11.7	13.4	10.8	11.3

Table 1: Material properties comparison. Solar transmission/infrared loss: measured. Infrared loss values before/after slash indicate pyrgeometer sensor/pane temperatures. Thermal conductivity: reference values [21–24] at 10-60 °C. Heat capacity: calculated for a 50 mm × 2 mm disk using reference density and specific heat values [25–29].

Pane	**Cond.**	**24hr**	**Peak Sun (12-3PM)**	**Direct Sun (8:30AM-6:30PM)**	**Indirect (6-8:30AM; 6:30-9PM)**	**Night (9PM-6AM)**
Boro	Sunny	+1.09	+2.61 $\pm$ 0.16	+2.07 $\pm$ 0.58	+0.48 $\pm$ 0.12	+0.43 $\pm$ 0.03
Sapphire	Sunny	+0.83	+0.50 $\pm$ 0.05	+0.72 $\pm$ 0.28	+0.97 $\pm$ 0.11	+0.86 $\pm$ 0.03
Boro	Cloudy	+0.73	+1.39 $\pm$ 0.29	+1.23 $\pm$ 0.44	+0.53 $\pm$ 0.14	+0.33 $\pm$ 0.12
Sapphire	Cloudy	+0.57	+0.18 $\pm$ 0.10	+0.41 $\pm$ 0.26	+0.87 $\pm$ 0.30	+0.57 $\pm$ 0.20

Table 2: Average temperature differences ($^\circ$C) $\pm$ 1 std (of 1-minute averages) between surfaces under infrared-opaque panes (borosilicate and sapphire) vs. infrared-transparent panes (CaF_2); data for both sunny (Figure 3) and cloudy (Figure 4) conditions.

Table 3: Heat Transfer Equations. Sign convention: $-$ for energy loss, $+$ for gain. Parameter values: $k_{\text{surf}} = 0.090$ W/(m·K) (PLA thermal conductivity), k_{air} = temperature-dependent air thermal conductivity, $S_{\text{cyl}} = 0.102$ m (housing shape factor), $A_{\text{pane}} = A_{\text{surf}} = \pi r_{\text{surf}}^2$ with $r_{\text{surf}} = 20$ mm, $\delta_{\text{gap}} = 1$ mm, $h_{\text{pane}} = 35$ W/(m^2·K) daytime / 20 W/(m^2·K) nighttime.

Mechanism	**Equation**
Conduction (surf → exterior air through apparatus housing)	$Q_{\text{cond,surf}\to\infty} = -k_{\text{surf}} \cdot S_{\text{cyl}} \cdot (T_{\text{surf}} - T_\infty)$
Conduction (surf → pane)	$Q_{\text{cond,surf}\to\text{pane}} = -k_{\text{air}} \cdot \frac{A_{\text{surf}}}{\delta_{\text{gap}}} \cdot (T_{\text{surf}} - T_{\text{pane}})$
Conduction (pane → surf)	$Q_{\text{cond,pane}\to\text{surf}} = -Q_{\text{cond,surf}\to\text{pane}}$
Convection (pane → exterior air)	$Q_{\text{conv,pane}\to\infty} = -h_{\text{pane}} \cdot A_{\text{pane}} \cdot (T_{\text{pane}} - T_\infty)$
Solar absorption (surf)	$Q_{\text{sun,surf}} = A_{\text{surf}} \cdot I_{\text{sun}} \cdot \tau_{\text{pane,sun}} \cdot \alpha_{\text{surf,sun}}$
Solar absorption (pane)	$Q_{\text{sun,pane}} = I_{\text{sun}} \cdot A_{\text{pane}} \cdot (\alpha_{\text{pane,sun}} + \tau_{\text{pane,sun}} \cdot \rho_{\text{surf,sun}})$
Radiant exitance	$M_i = \varepsilon_i \sigma T_i^4$
Radiative exchange (surf ↔ other ∈ {panewall, topwall, sky}): • surface emission • absorption of pane emission • transmitted emission (sky, walls) • reflection of surf emission off pane	$Q_{\text{rad,surf}} = \sum_{\text{other}} F_{\text{surf}\to\text{other}} \cdot A_{\text{surf}} \big[$ $- M_{\text{surf}}$ $+ \varepsilon_{\text{surf}} M_{\text{pane}}$ $+ \varepsilon_{\text{surf}} \tau_{\text{pane,ir}} M_{\text{other}}$ $+ \rho_{\text{pane,ir}} M_{\text{surf}}$ $\big]$
Radiative exchange (pane ↔ wall): • pane emission • absorption of wall emission • reflection of sky off wall	$Q_{\text{rad,toppane}} = F_{\text{toppane}\to\text{topwall}} \cdot A_{\text{pane}} \big[$ $- M_{\text{pane}}$ $+ \varepsilon_{\text{pane}} M_{\text{topwall}}$ $+ \rho_{\text{topwall,ir}} \varepsilon_{\text{pane}} I_{\text{sky}}$
Radiative exchange (pane ↔ sky): • pane emission • absorption of sky backradiation	$\big] + F_{\text{toppane}\to\text{sky}} \cdot A_{\text{pane}} \big[$ $- M_{\text{pane}}$ $+ \varepsilon_{\text{pane}} I_{\text{sky}}$ $\big]$
Radiative exchange (pane ↔ surf): • pane emission • absorption of surface emission • reflection of pane emission off surface	$Q_{\text{rad,botpane}} = A_{\text{pane}} \big[$ $- M_{\text{pane}}$ $+ \varepsilon_{\text{pane}} M_{\text{surf}}$ $+ \rho_{\text{surf,ir}} M_{\text{pane}}$ $\big]$

Table 4: Steady-State Model Results. Comparison of measured and modeled surface temperatures with detailed heat flow analysis. $Q^\circ = Q/A$.

	Peak Sunlight			**Nighttime**			**Units**
T_∞		30.2			16.2		°C
I_{sun}		855.7			0.0		W/m^2
I_{sky}		371.8			324.4		W/m^2
	Boro	**Sapph**	**CaF$_2$**	**Boro**	**Sapph**	**CaF$_2$**	
T_{pane} (model)	44.94	43.67	43.27	14.28	14.71	14.47	°C
T_{surf} (model)	60.06	58.21	57.59	14.66	15.00	14.34	
vs. CaF$_2$	+2.48	+0.62	–	+0.33	+0.67	–	
T_{surf} (real)	58.70	56.60	55.60	14.80	15.30	14.40	°C
vs. CaF$_2$	+3.10	+1.00	–	+0.40	+0.90	–	
$Q^\circ_{\text{cond,surf}\to\infty}$	−218.7	−205.1	−200.6	11.3	8.8	13.7	W/m^2
$Q^\circ_{\text{cond,surf}\to\text{pane}}$	−416.3	−398.6	−392.1	−9.5	−7.3	3.4	
$Q^\circ_{\text{sun,surf}}$	735.7	676.4	743.0	0.0	0.0	0.0	
$Q^\circ_{\text{rad,surf}}$	−100.7	−72.6	−150.4	−1.8	−1.5	−17.0	
$Q^\circ_{\text{rad,surf}\to\text{emit}}$	−631.7	−617.7	−613.1	−351.6	−353.3	−350.0	
$Q^\circ_{\text{rad,surf}\leftarrow\text{pane}}$	493.1	356.2	292.8	328.7	242.8	199.9	
$Q^\circ_{\text{rad,surf}\leftarrow\text{refl}}$	37.9	185.3	36.8	21.1	106.0	21.0	
$Q^\circ_{\text{rad,surf}\leftarrow\text{other}}$	0.0	3.6	133.2	0.0	3.0	112.1	
$Q^\circ_{\text{cond,pane}\leftarrow\text{surf}}$	416.3	398.6	392.1	9.5	7.3	−3.4	W/m^2
$Q^\circ_{\text{conv,pane}\to\infty}$	−442.3	−404.1	−392.0	38.4	29.8	34.5	
$Q^\circ_{\text{sun,pane}}$	102.9	59.6	44.2	0.0	0.0	0.0	
$Q^\circ_{\text{rad,pane}}$	−76.9	−54.1	−44.3	−47.9	−37.1	−31.2	
$Q^\circ_{\text{rad,botpane}}$	103.5	71.6	55.7	0.0	0.0	0.0	
$Q^\circ_{\text{rad,toppane}}$	−183.0	−127.3	−103.5	−47.8	−39.8	−31.8	